Electronic Supplementary Information

Mo-doping heterojunction: interfacial engineering in an efficient electrocatalyst toward superior simulated seawater hydrogen evolution

Zuo-Ming He [†] [a,b], Chun-Xiao Zhang [†] [d], Si-Qi Guo [†] [e], Peng Xu[a], Yuan Ji[a], Si-Wei Luo[a], Xiang Qi[a], Yun-Dan Liu[a], Ning-Yan Cheng*[e], Shi-Xue Dou[f], Yun-Xiao Wang*[f,g], Bin-Wei Zhang*[b,c]*

[a] *Hunan Key Laboratory of Micro-Nano Energy Materials and Devices, Xiangtan University; Xiangtan 411105, P. R. China*

E-mail: liuyd@xtu.edu.cn

[b] *School of Chemistry and Chemical Engineering, Chongqing University, Chongqing 400044, P. R. China E-mail: binwei@cqu.edu.cn*

[c] *Center of Advanced Electrochemical Energy, Institute of Advanced Interdisciplinary Studies, Chongqing 400044, P. R. China*

[d] *School of Physics and Optoelectronic Engineering, Shandong University of Technology, Zibo 255000, P. R. China*

[e] *Materials and Intelligent Sensing Laboratory of Anhui Province, Key Laboratory of Structure and Functional Regulation of Hybrid Materials of Ministry of Education, Institutes of Physical Science and Information Technology, Anhui University, Hefei 230601, P. R. China*

E-mail: ningyancheng@ahu.edu.cn

[f] *Institute of Energy Materials Science (IEMS), University of Shanghai For Science and Technology, 516 Jungong Road, Shanghai, 200093, China*

[g] *Institute for Superconducting and Electronic Materials, Australian Institute of Innovative Materials, University of Wollongong, Innovation Campus, Squires Way, North Wollongong, New South Wales 2500, Australia*

E-mail: yunxiao@uow.edu.cn

† . These authors contributed equally: Z. M. He, C. X. Zhang, S. Q. Guo

1. Experimental Procedures

1.1. Materials.

Carbon cloth was provided by a commercial supplier (CeTech Co., Ltd), and $Ni(CH_3COO)_2 \cdot 4H_2O$, ammonium molybdate tetrahydrate, $CO(NH_2)_2$, $NaBH_4$, $Na_2MoO_4 \cdot 2H_2O$, and selenium powder were purchased from Aladdin Co., Inc.20 wt.% Pt/C and 5 wt. % Nafion were purchased from Sigma–Aldrich. All the other reagents were analytical grade and used in the synthesis process as received without further purification.

1.2. Characterization.

X-ray diffraction (XRD) patterns were recorded on a Rigaku D/Max 2500V instrument with Cu Kα radiation in the 2θ range of 10-80°. The morphology of the samples was investigated by scanning electron microscopy (SEM, JEOLJSM-6360). Scanning transmission electron microscopy (STEM) images and energy-dispersive X-ray spectroscopy (EDS) data were acquired on a JEOL NEOARM200F microscope equipped with a spherical aberration (Cs) probe corrector at 200 kV. X-ray photoelectron spectroscopy (XPS) was conducted on a Kratos Analytical Ltd instrument with a Cu Kα source. Raman spectra were recorded on an WITec Raman microscope with an excitation laser wavelength of 532 nm.

1.3. Electrochemical measurement

Electrochemical measurements were conducted on an electrochemical work station (CHI660D) with a typical three-electrode electrochemical cell consisting of a reference electrode (a Hg/HgO electrode), a counter electrode (carbon rod), and the working electrode. for electrochemical tests in alkaline high-purity water, a 1 M KOH solution was used as the electrolyte. For the electrochemical tests in alkaline simulated seawater, a mixture solution containing 1 M KOH and 0.5 M NaCl were used as electrolyte.

Before the test, the catalyst was subjected to CV at a scan rate of 50 mV/s to stabilize and activate the it. The electro-catalytic HER properties were measured using linear sweep voltammetry (LSV) at a scan rate of 2 mV/s. All of the LSV curves have been corrected for IR compensation. Electrochemical impedance spectroscopy (EIS) was performed at an overpotential of 250 mV vs. RHE in the frequency range 10^{-1}~10^{5} Hz. To estimate the electrochemical surface area, C_{dl} values were obtained by scanning CVs in the non-ohmic potential range of 0.0254~0.125 V vs. RHE with scan rates from 20 to 180 mV/s.

1.4. Computational details

First-principles calculations were performed using the Vienna Ab initio Simulation Package (VASP) based on density functional theory (DFT)[1-3]. Both structural relaxation and static self-consistency calculations employed the generalized gradient approximation (GGA) with Perdew-Burke-Ernzerhof (PBE)[4]. The interaction of ions with electrons was ascribed by projector-augmented wave potentials (PAWs)[5]. The cutoff energy was set to 500 eV. The convergence precision for energy and force was set at 10^{-5} eV and 0.01 eV $Å^{-1}$ per atom, respectively. A dipole correction was applied for the entire calculation because of the asymmetry in the vertical direction[6, 7]. A six-layer-thick of NiSe supercell (96 atoms) was used to simulate the surface reactions, and a vertical vacuum layer of over 20 Å was set to separate the neighboring layers.

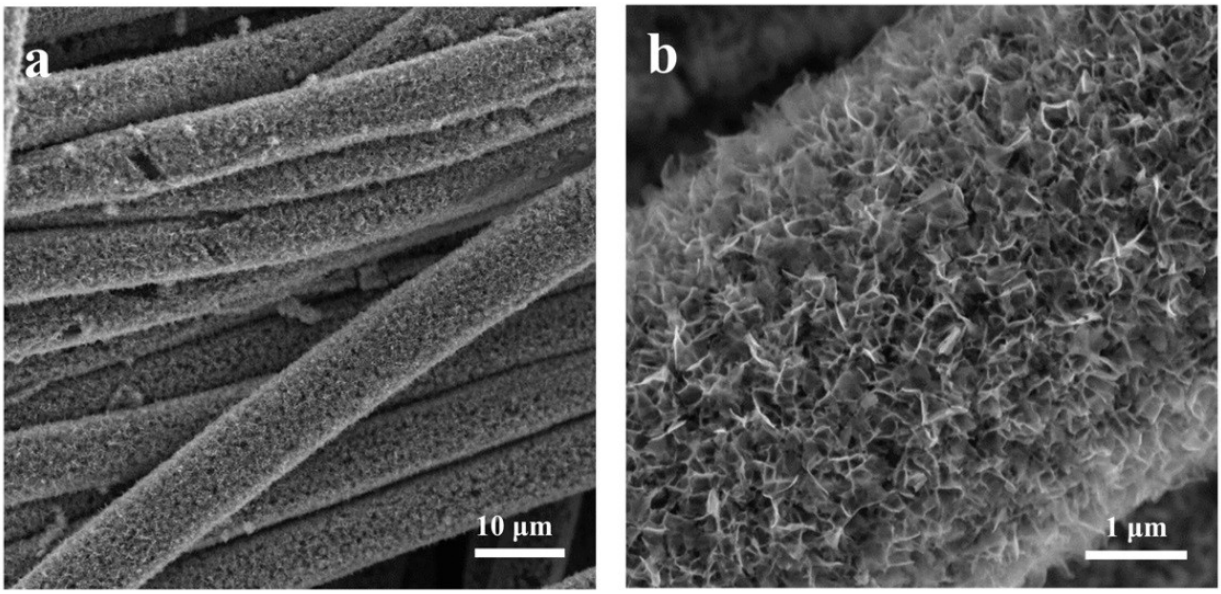

Figure S1. SEM images of $NiMoO_4$ on CC.

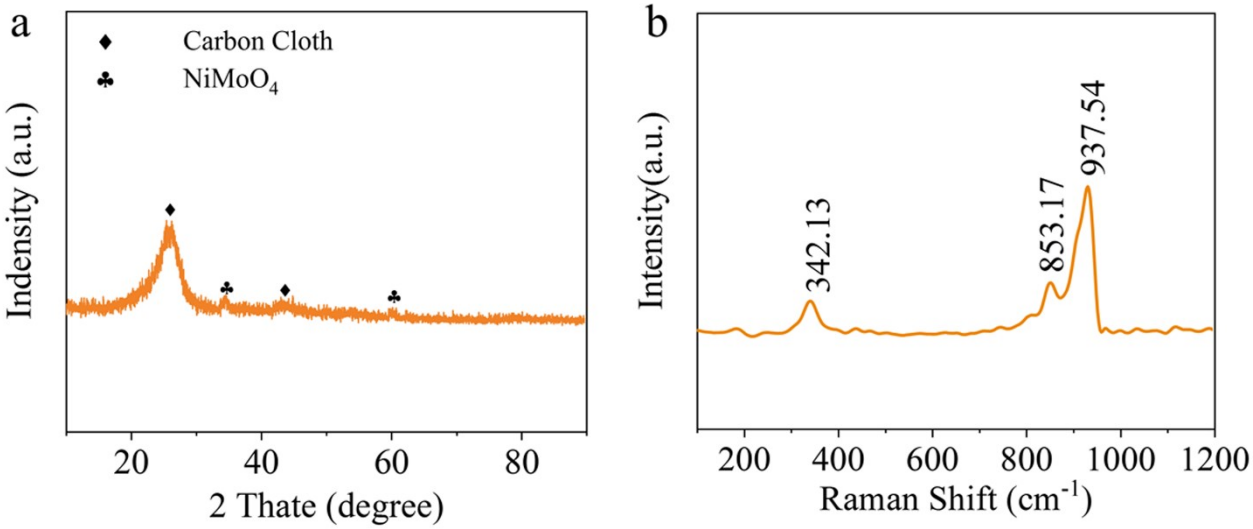

Figure S2. XRD pattern and Raman spectrum of $NiMoO_4$ precursor.

There is no obvious characteristic peak of the $NiMoO_4$ precursor in the XRD pattern, indicating its low crystallinity.

The Raman spectra show the peaks at 342.13, 853.17 and 937.54 cm^{-1}, which may correspond to the bending mode of Mo–O, the stretching vibrations of the bridging Mo–O–M bonds (M=Ni or Mo) and Mo=O bonds of $NiMoO_4$, respectively.

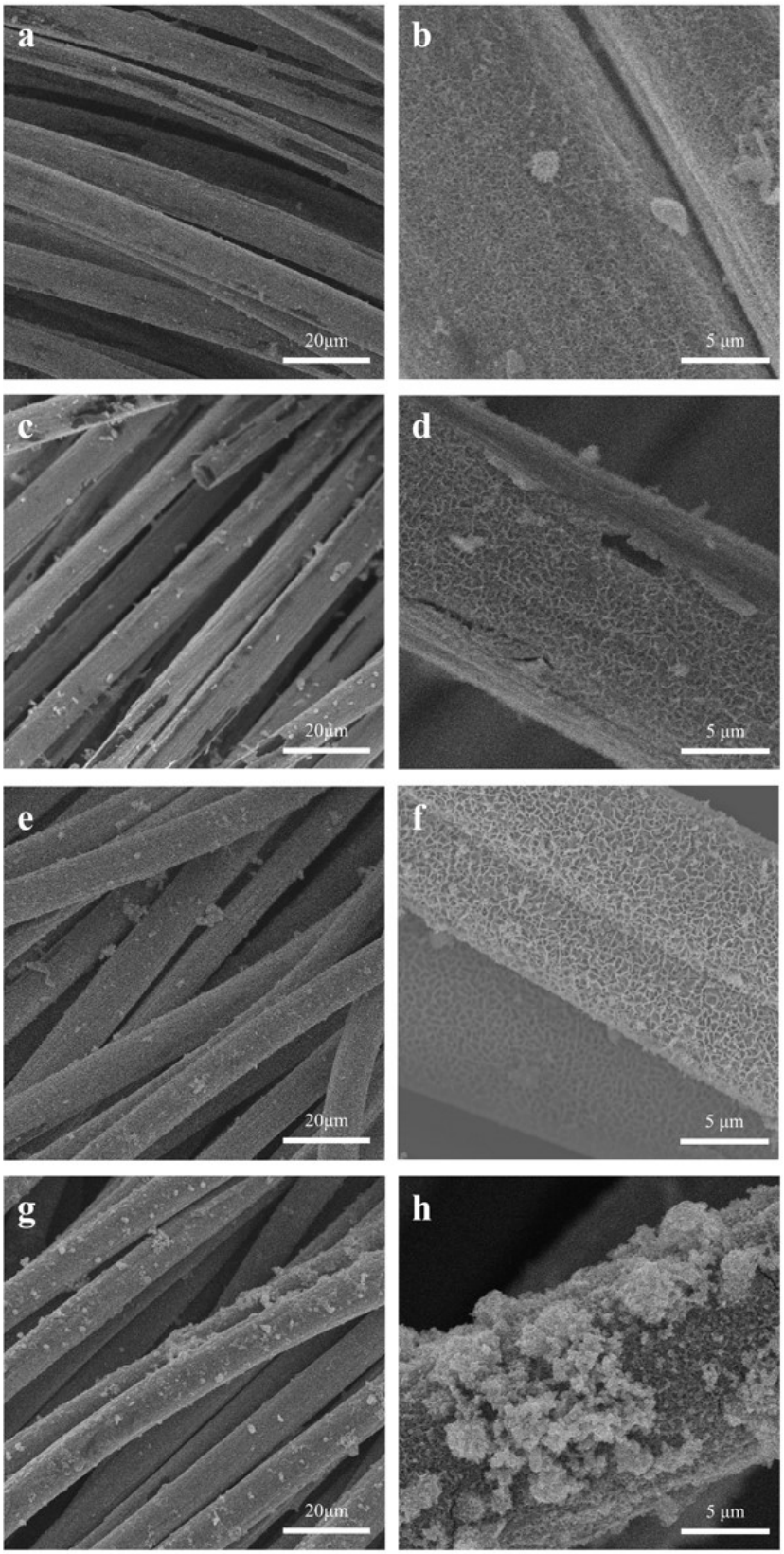

Figure S3. SEM images of (a-b) Mo_x-$Ni_{0.85}Se/MoSe_2$-10, (c-d) Mo_x-$Ni_{0.85}Se/MoSe_2$-30, (e-f) Mo_x-$Ni_{0.85}Se/MoSe_2$, (g-h) Mo_x-$Ni_{0.85}Se/MoSe_2$-90.

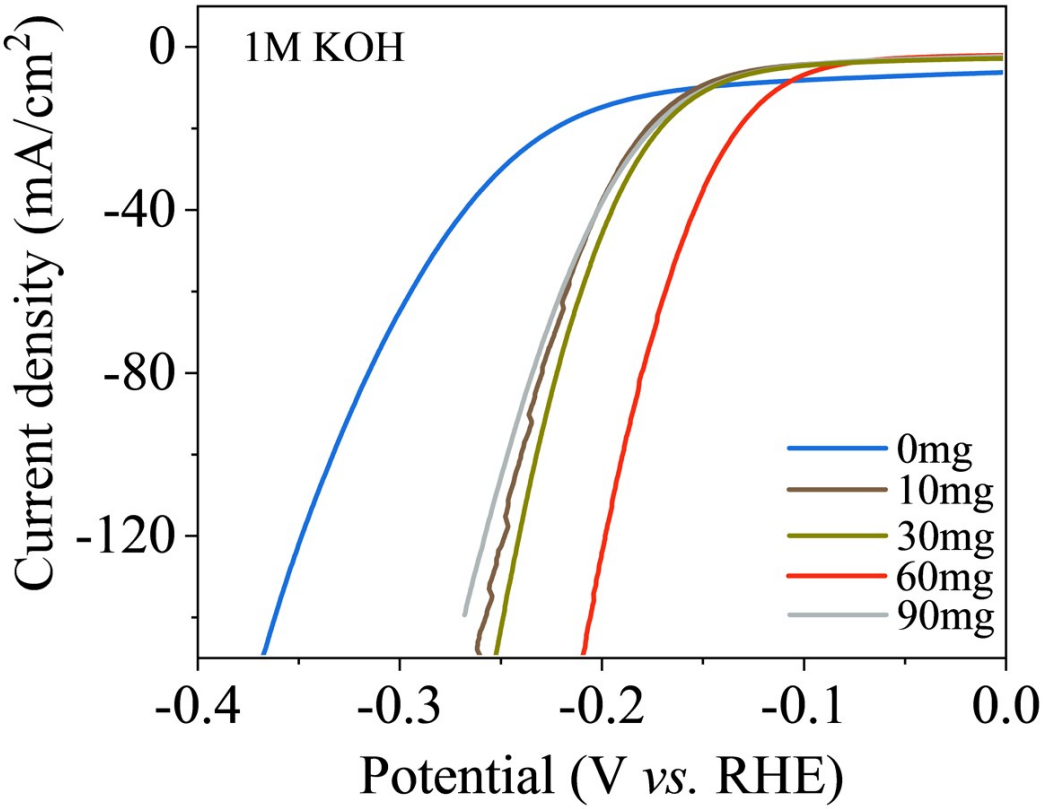

Figure S4. The HER polarization curves of a series of Mo_x-$Ni_{0.85}Se/MoSe_2$, which were prepared with different amounts of $NaMoO_4 \cdot 2H_2O$, in 1 M KOH solution.

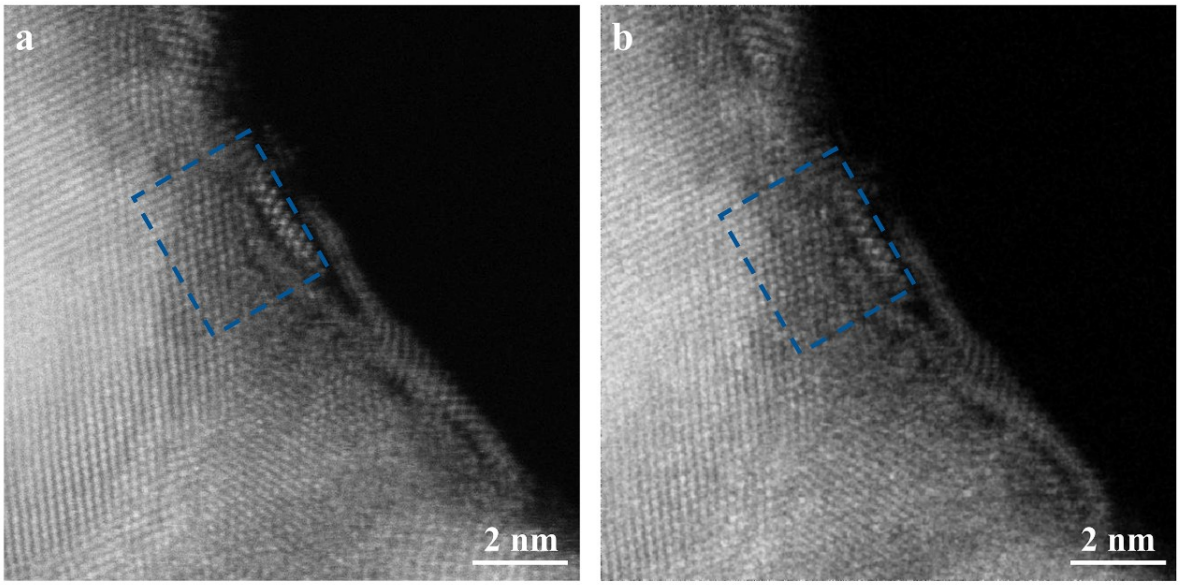

Figure S5. HAADF-STEM images of Mo_x-$Ni_{0.85}Se/MoSe_2$ with different defocus in the same area.

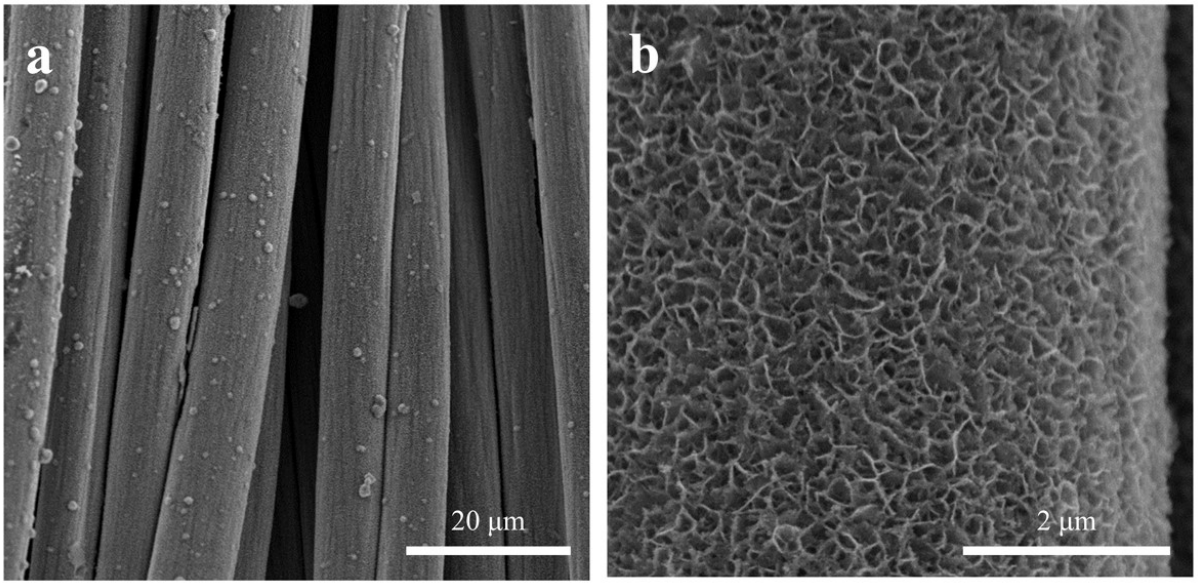

Figure S6. SEM images of $NiSe_2$ on CC.

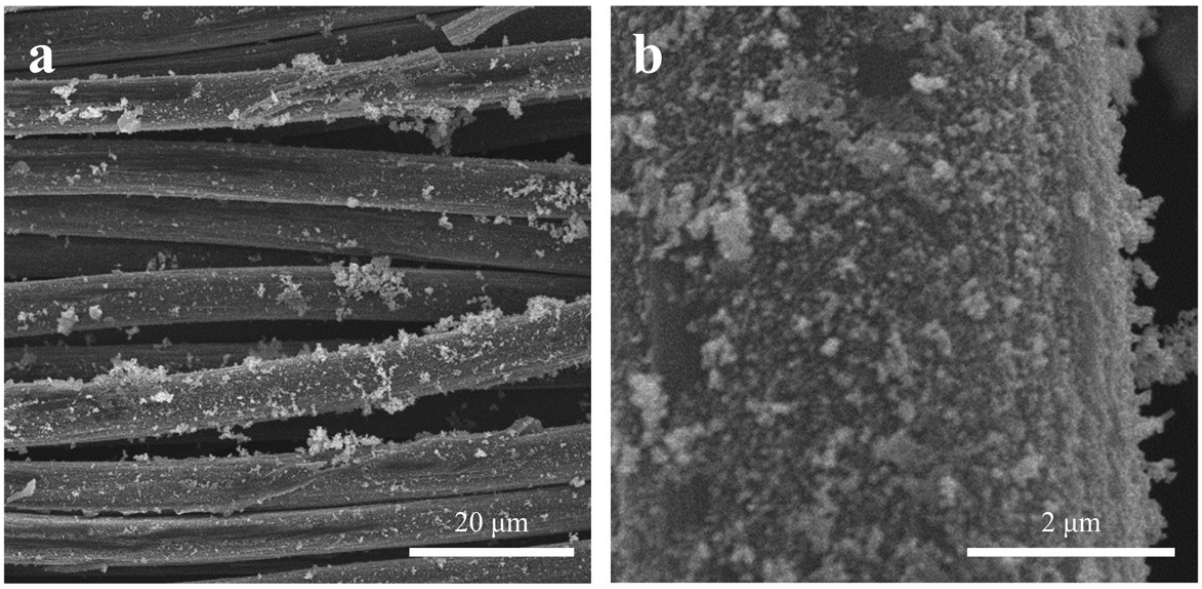

Figure S7. SEM images of $MoSe_2$ on CC.

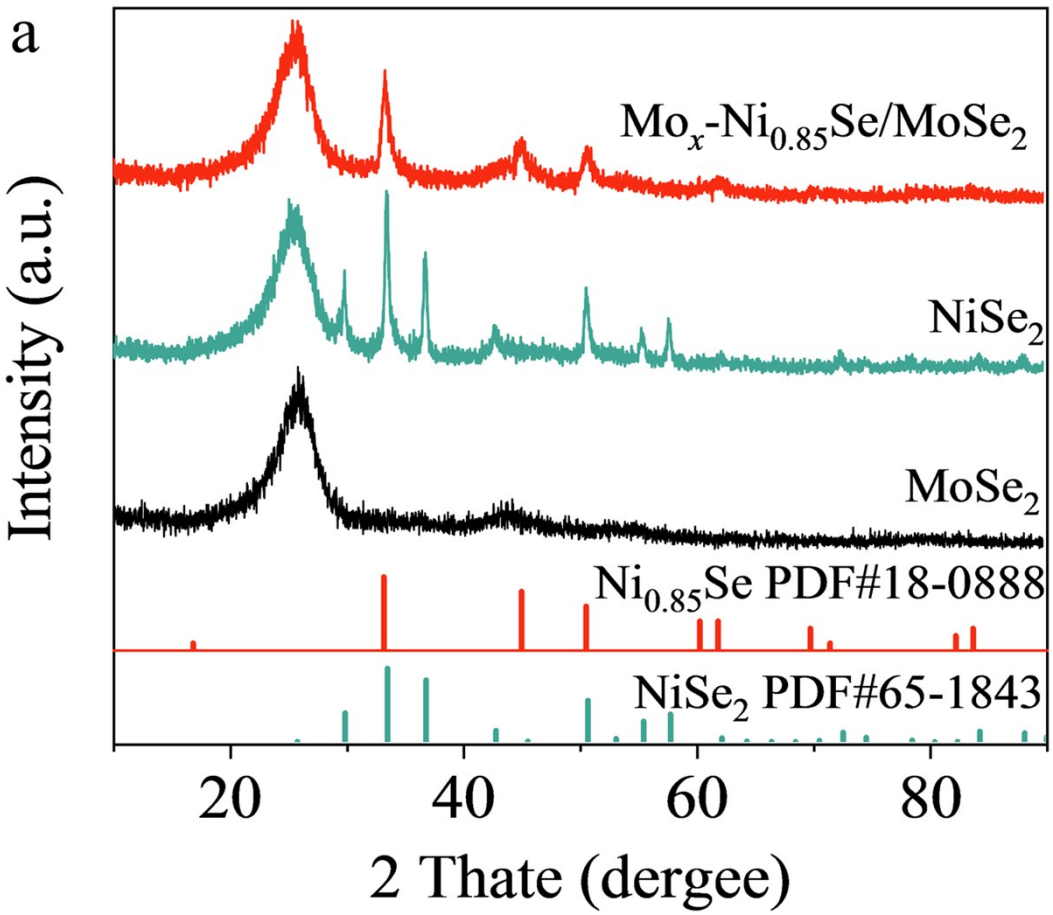

Figure S8. XRD patterns of Mo_x-$Ni_{0.85}Se/MoSe_2$, $MoSe_2$, and $NiSe_2$. It should be noted that the two distinct peaks sitting around 26° and 43° originate from the carbon cloth substrate.

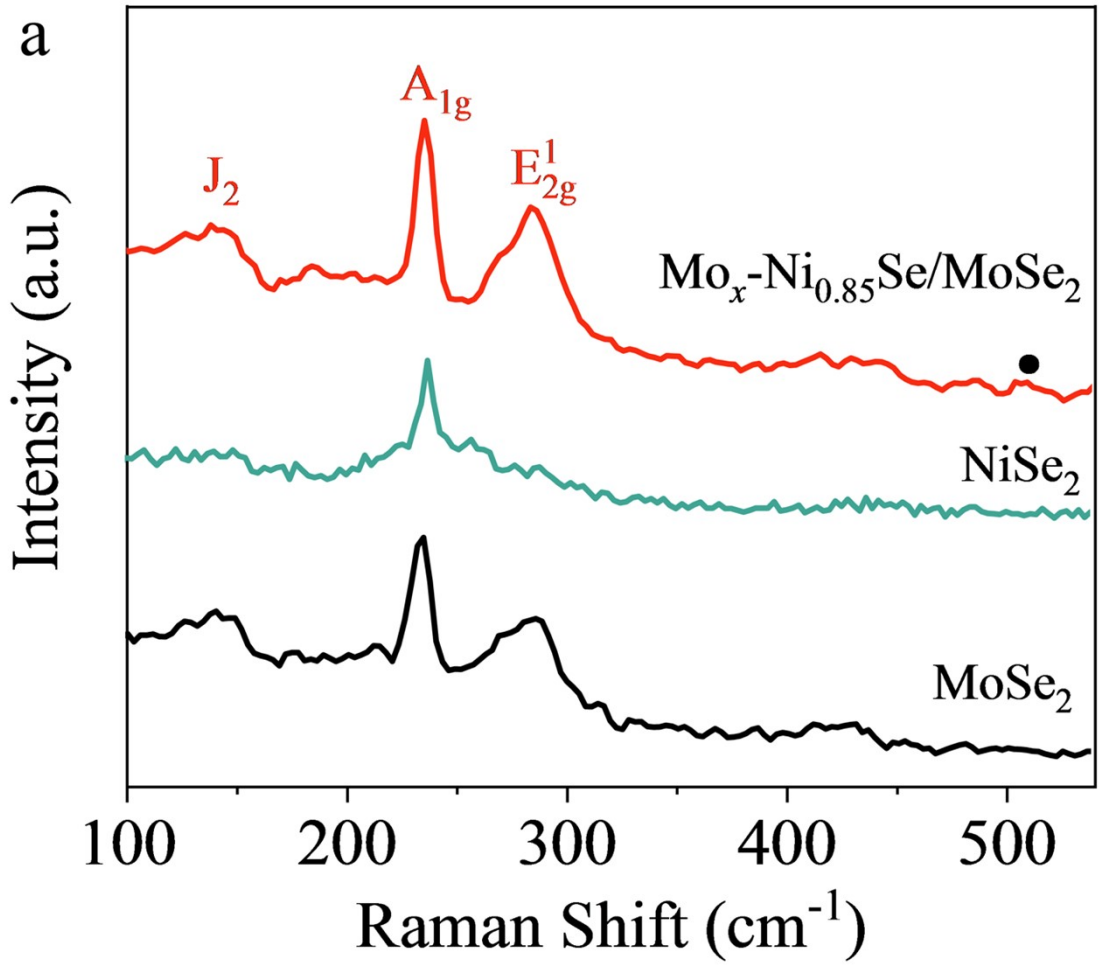

Figure S9. Raman spectra of Mo_x-$Ni_{0.85}Se/MoSe_2$, $MoSe_2$, and $NiSe_2$.

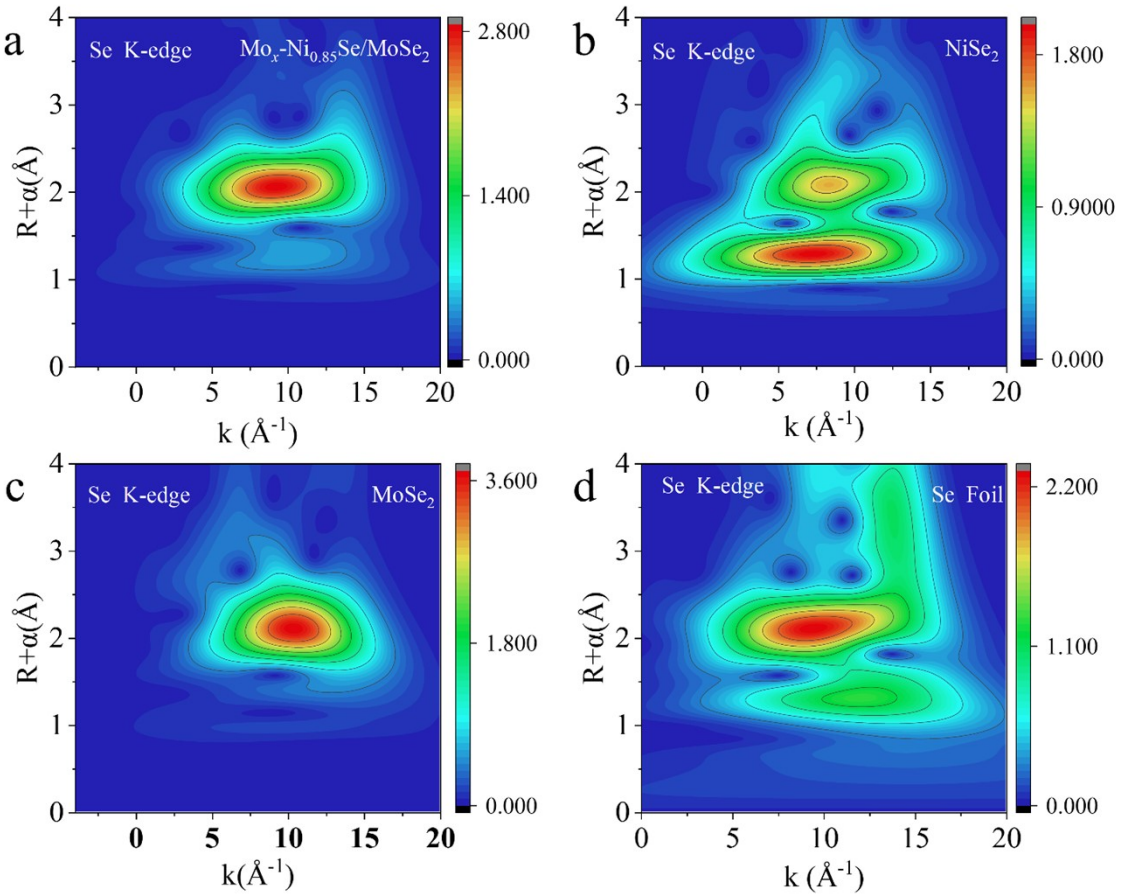

Figure S10. Wavelet transform of Se K-edge EXAFS for Mo$_x$-Ni$_{0.85}$Se/MoSe$_2$, NiSe$_2$, MoSe$_2$, and Ni Foil. The Se wavelet transform-EXAFS indicates the Ni-Se coordination in Mo$_x$-Ni$_{0.85}$Se/MoSe$_2$ shares a similar coordination environment to that of NiSe$_2$ and MoSe$_2$.

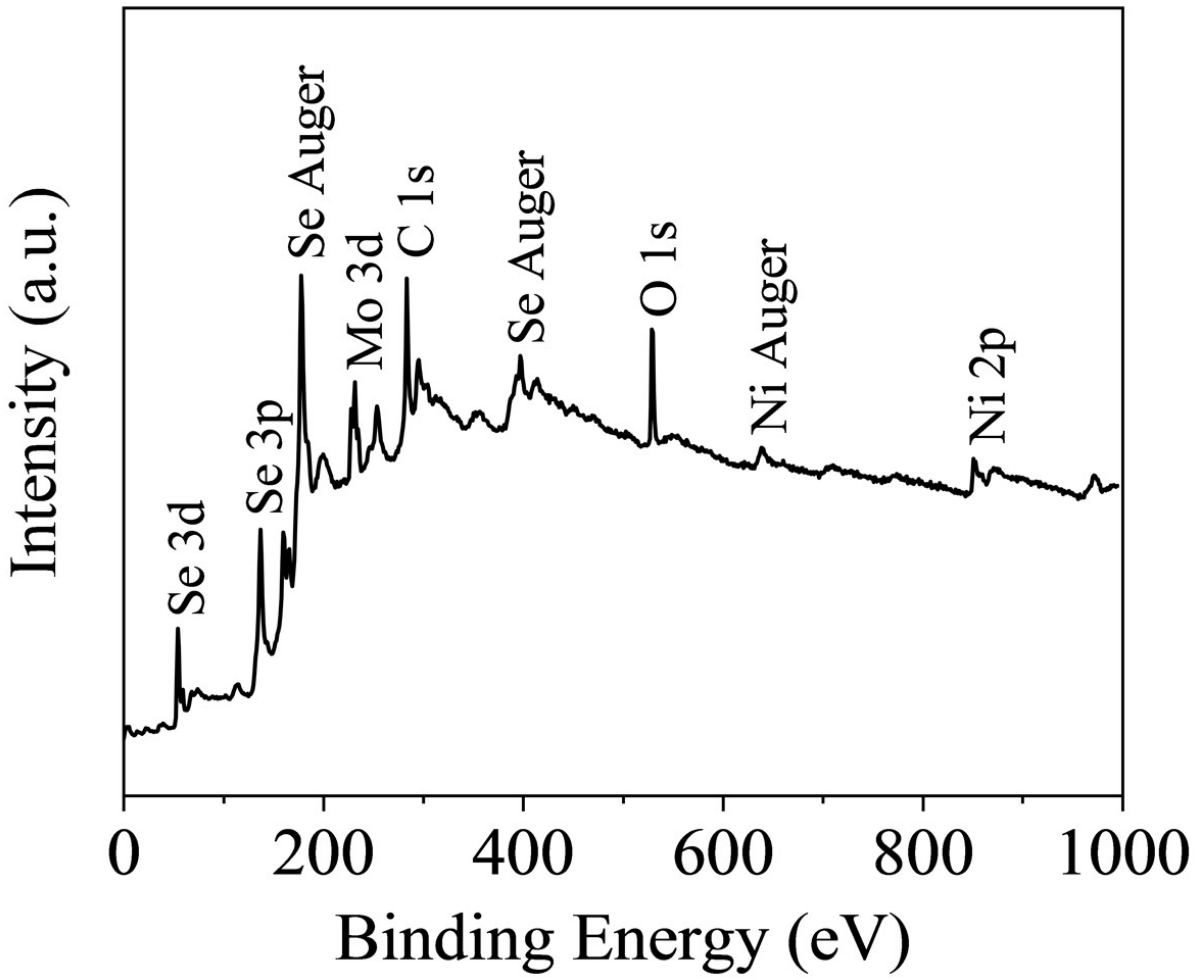

Figure S11. The XPS survey spectrum of Mo_x-$Ni_{0.85}Se/MoSe_2$.

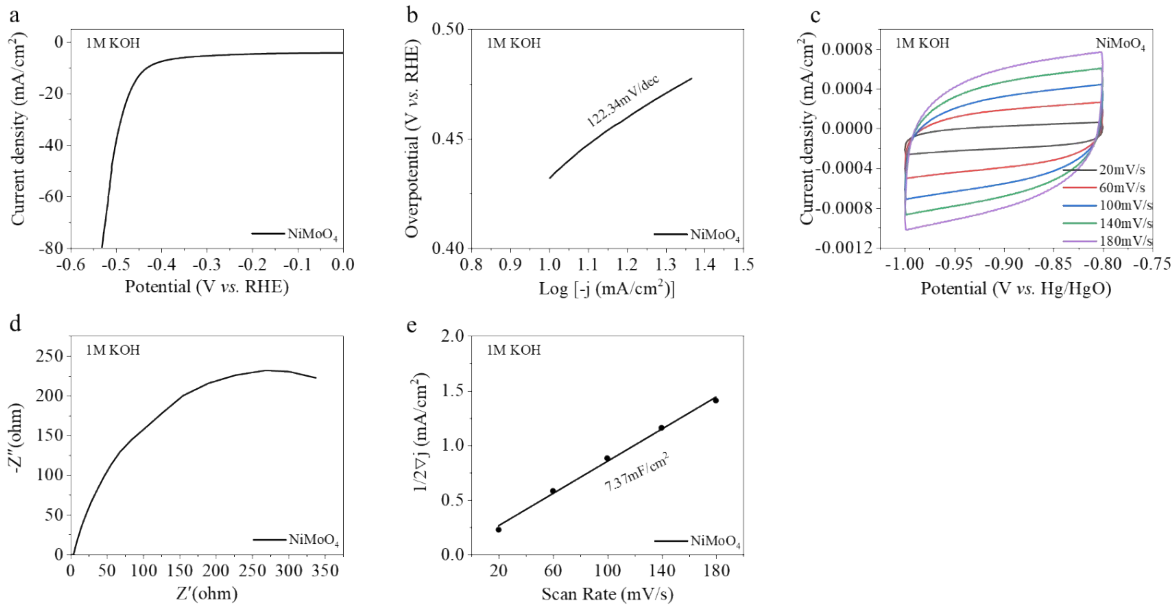

Figure S12. (a) The LSV curve, (b) the Tafel slope curve, (c) CV curves with different scan rates, (d) the EIS curve, and (e) the capacitive currents at -0.5 V vs. RHE as a function of scan rate for $NiMoO_4$ in 1 M KOH.

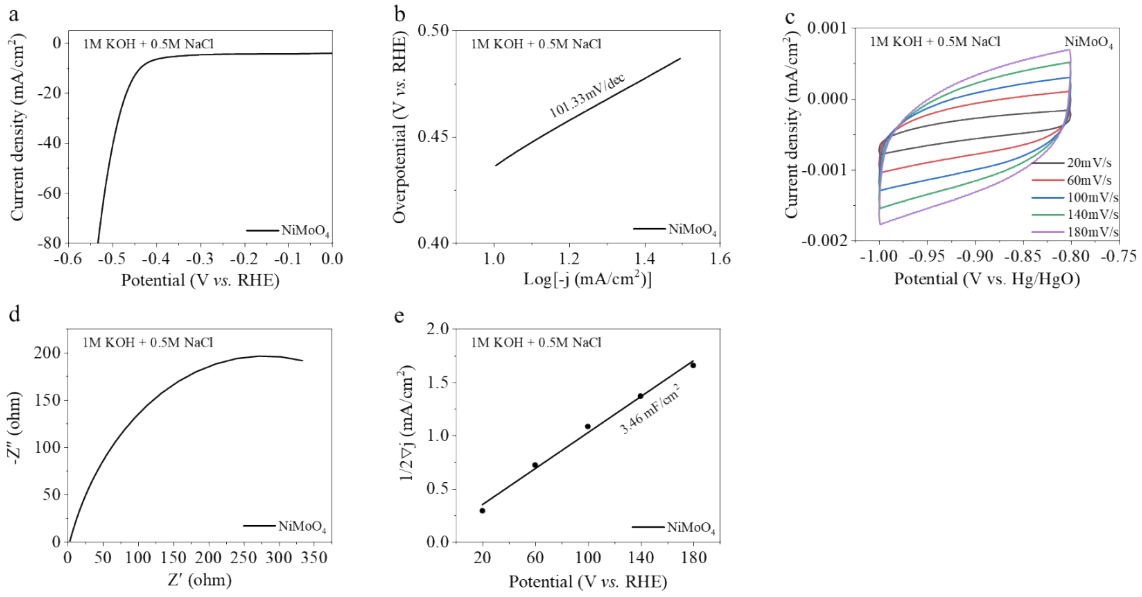

Figure S13. (a) The LSV curve, (b) Tafel slope curve, (c) CV curves with different scan rates, and (d) EIS curve of $NiMoO_4$ in simulated alkaline seawater. (e) Capacitive currents at -0.5 V vs. RHE as a function of scan rate for $NiMoO_4$ in simulated alkaline seawater.

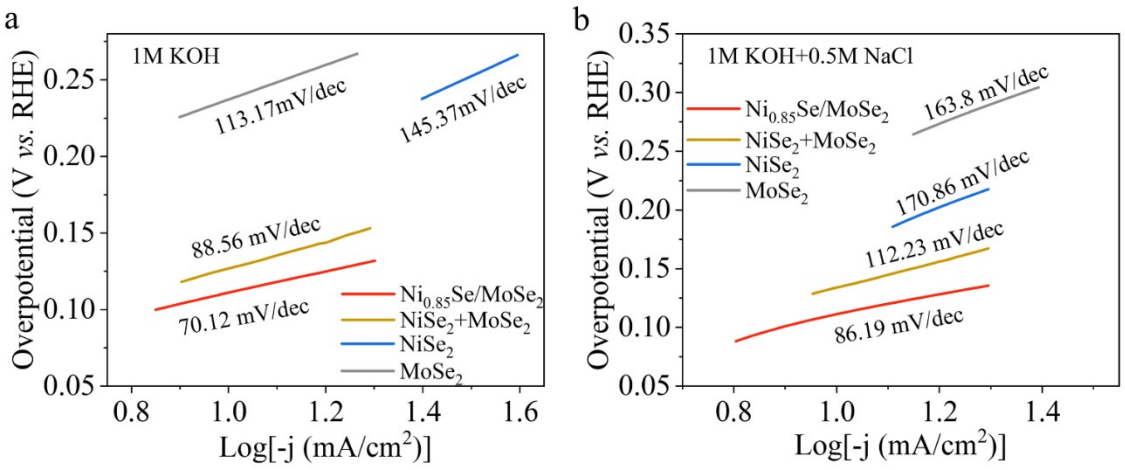

Figure S14. Tafel slopes of Mo_x-$Ni_{0.85}Se/MoSe_2$, $NiSe_2$+$MoSe_2$, $NiSe_2$, and $MoSe_2$ in (a) 1 M KOH and (b) in alkaline simulated seawater (1 M KOH + 0.5 M NaCl), respectively.

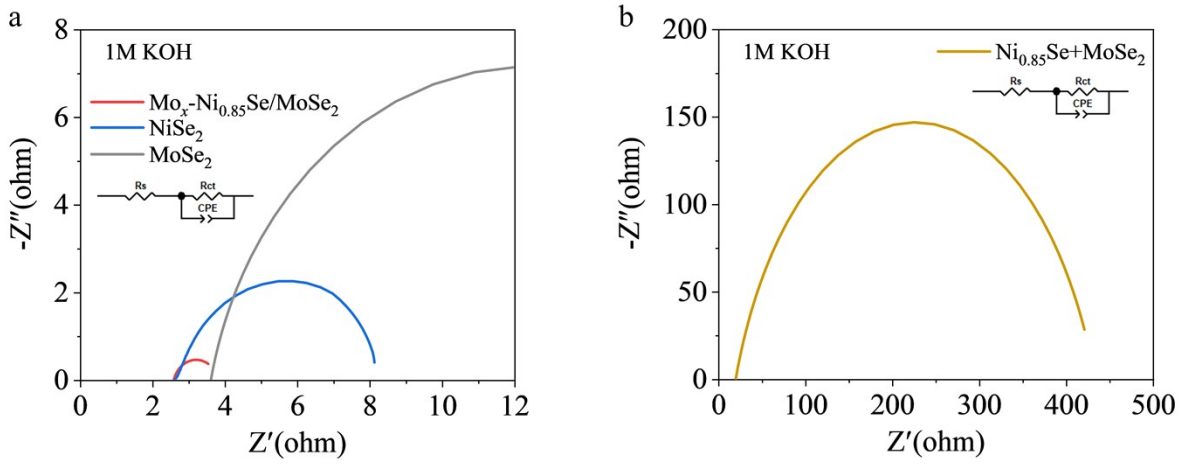

Figure S15. (a) The EIS curve (with inset equivalent circuit) of Mo_x-$Ni_{0.85}Se/MoSe_2$, $NiSe_2$, $MoSe_2$ and (b) physical mixed sample in 1 M KOH.

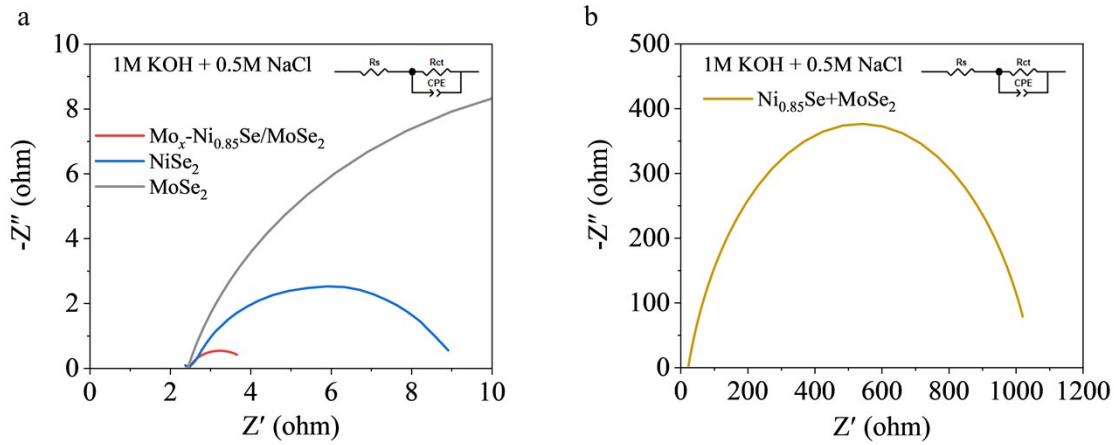

Figure S16. (a) The EIS curve (with inset equivalent circuit) of Mo_x-$Ni_{0.85}Se/MoSe_2$, $NiSe_2$, $MoSe_2$ and (b) physical mixed sample in alkaline simulated seawater.

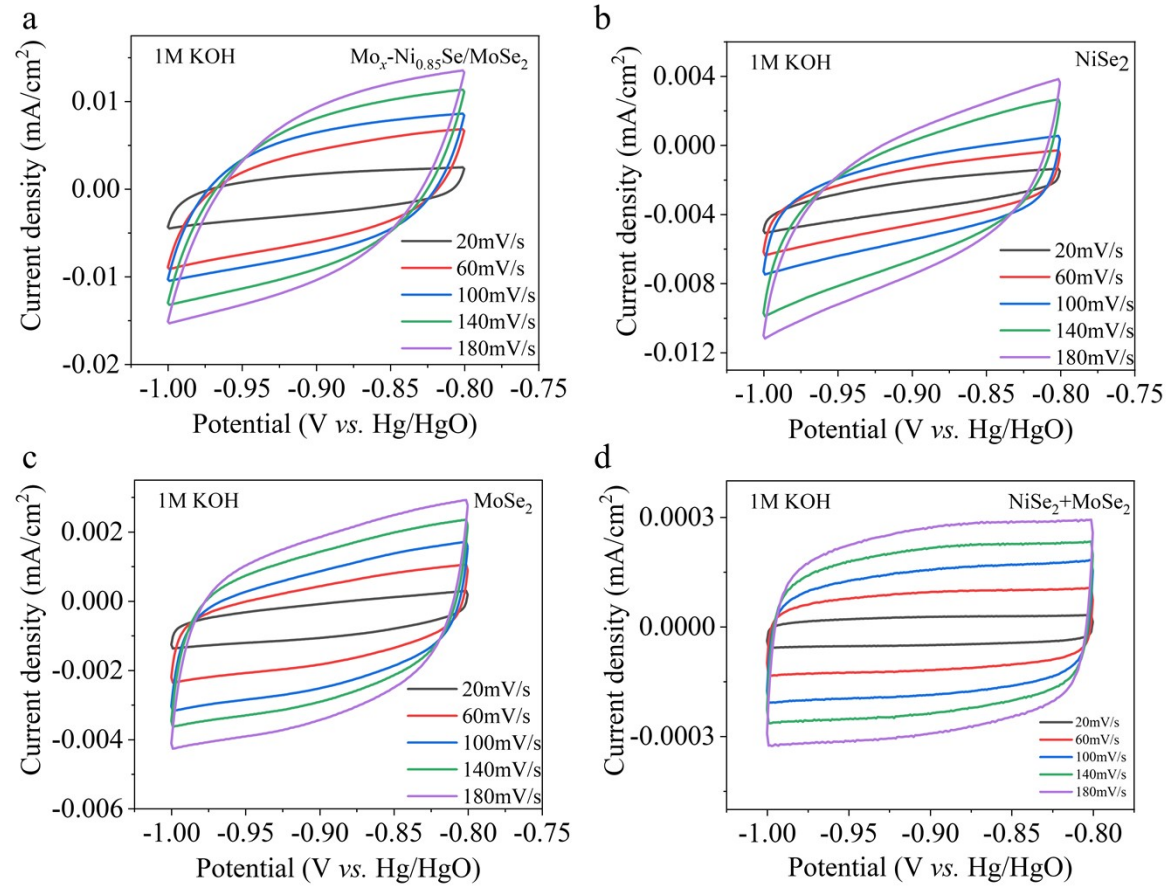

Figure S17. The CV curve of (a) Mo_x-$Ni_{0.85}Se/MoSe_2$, (b) $NiSe_2$, (c) $MoSe_2$, (d) $NiSe_2$+$MoSe_2$ in 1 M KOH.

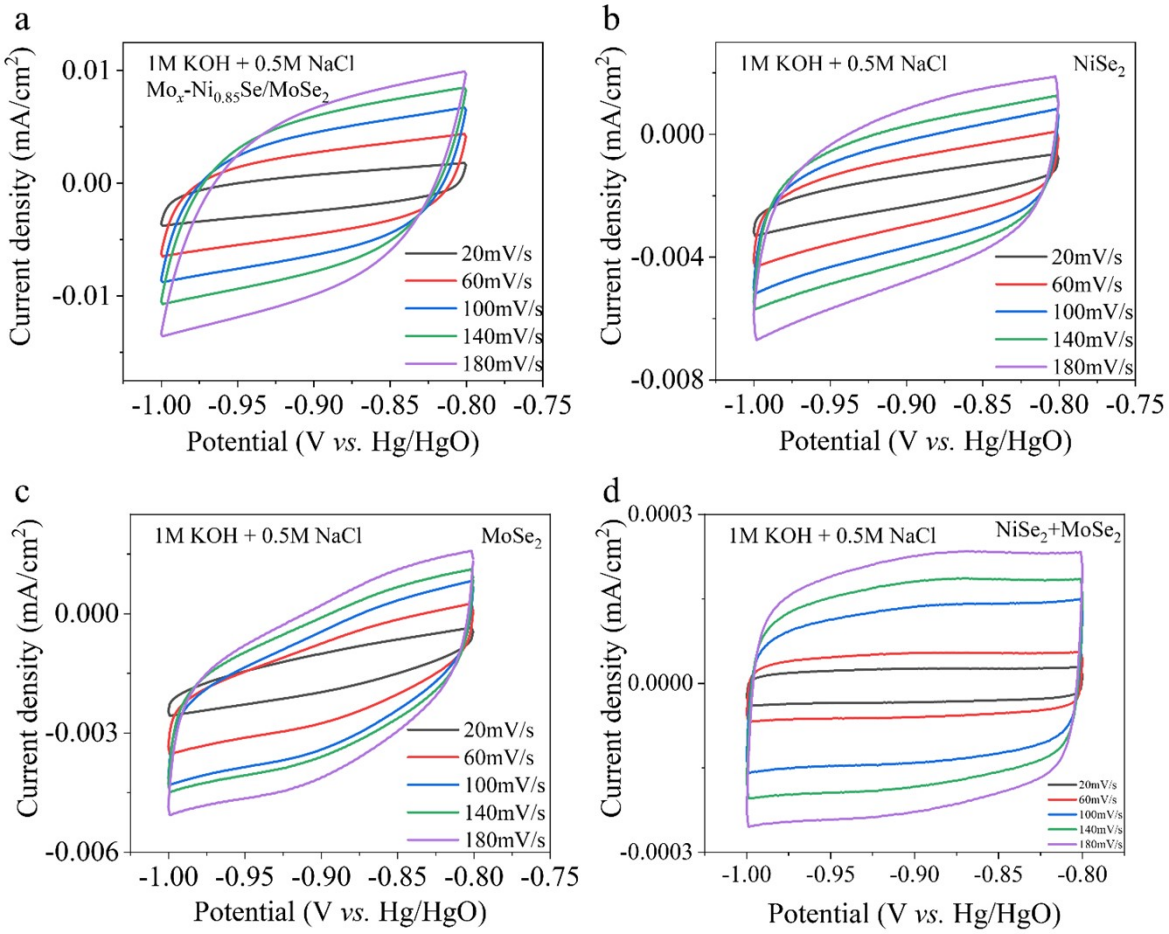

Figure S18. The CV curve of (a) Mo_x-$Ni_{0.85}Se/MoSe_2$, (b) $NiSe_2$, (c) $MoSe_2$, (d) $NiSe_2$+$MoSe_2$ in alkaline simulated seawater.

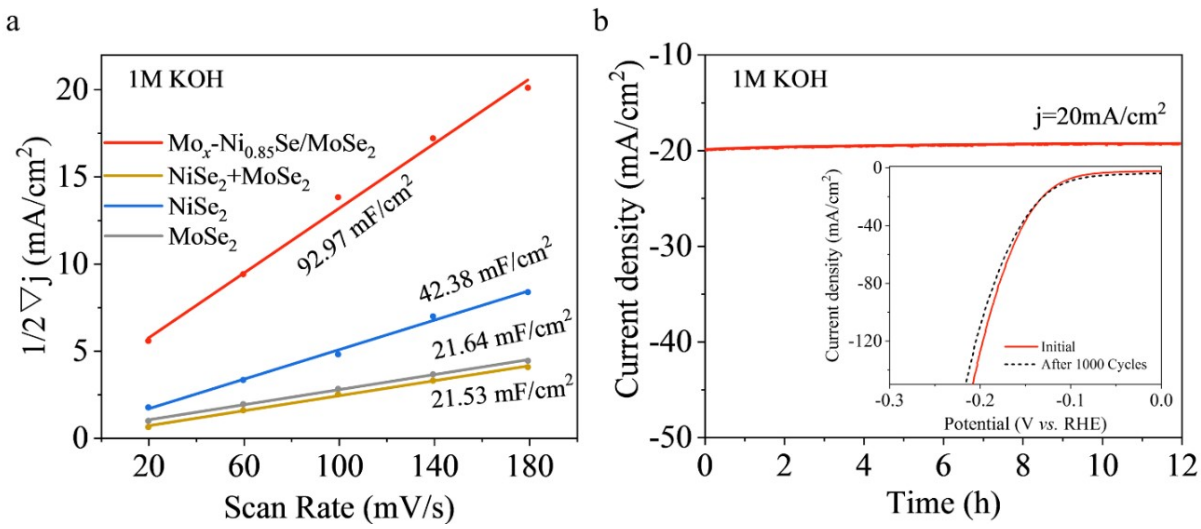

Figure S19. (a) Electrochemically active surface area (ECSA) and versus double-layer capacitance (Cdl), (b) Chronopotentiometry test of Mo_x-$Ni_{0.85}Se/MoSe_2$ catalyst at 20 mA /cm^2 for 12 h (inset: LSV curves before and after 1000 cycles of CV) in 1 M KOH.

The durability test results of Mo_x-$Ni_{0.85}Se/MoSe_2$ (Supplementary Figure 19b) reveal that it exhibits superior electrochemical stability as it can stably run 12 h at 20 mA/cm^2 in 1 M KOH with negligible current density drop.

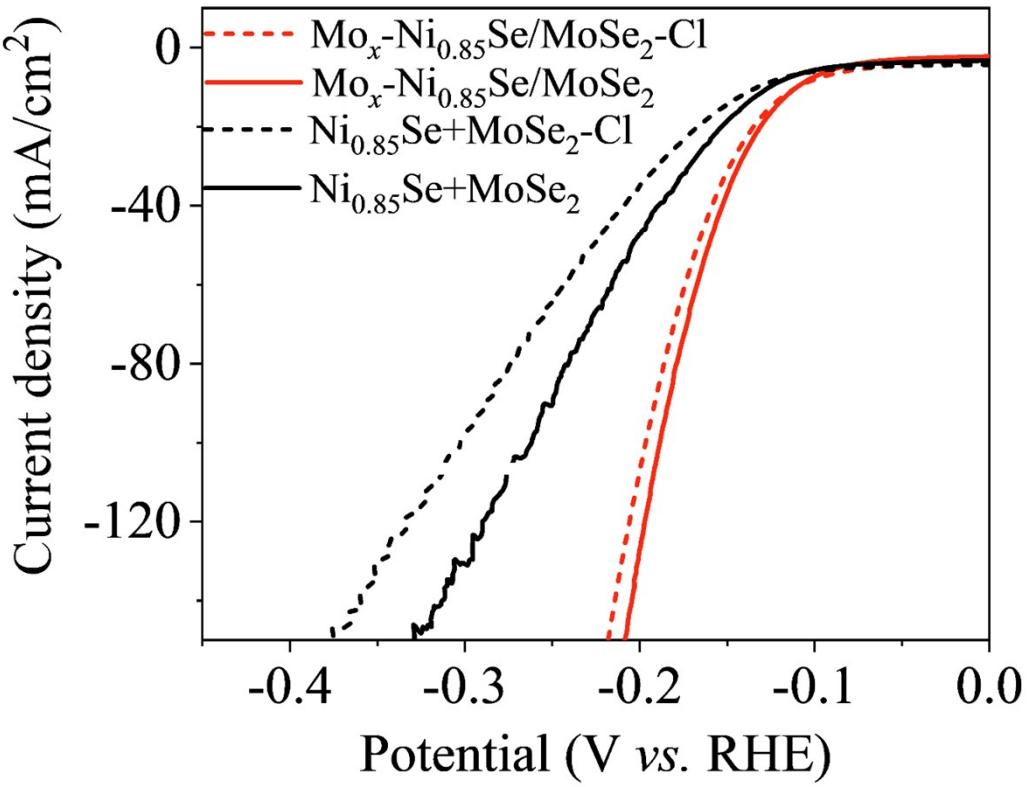

Figure S20. Polarization curves of Mo$_x$-Ni$_{0.85}$Se/MoSe$_2$ and Physical mixed sample (marked as Ni$_{0.85}$Se+MoSe$_2$) in 1 M KOH and alkaline simulated seawater (Cl representative in alkaline simulated seawater).

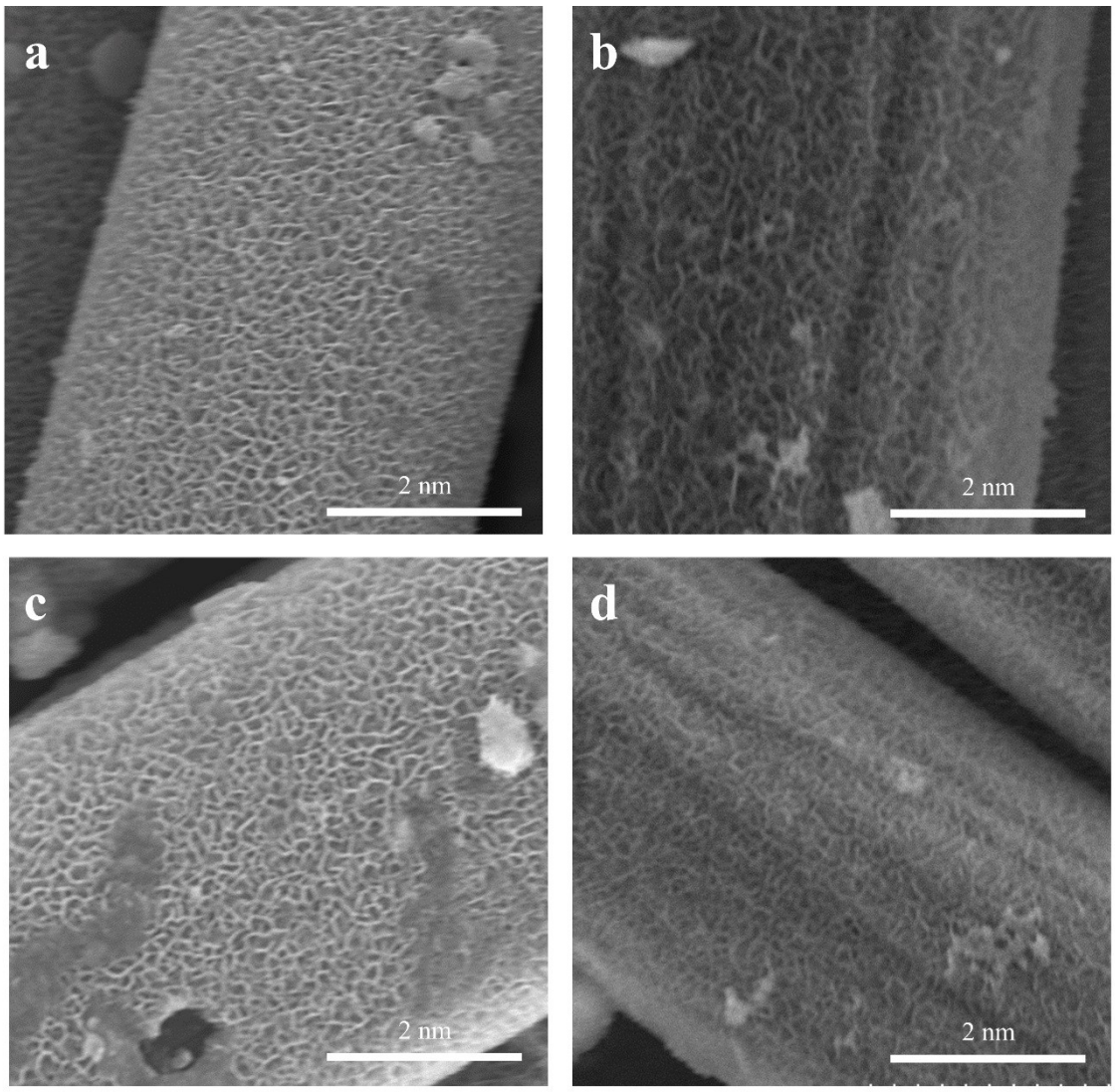

Figure S21. SEM images of Mo_x-$Ni_{0.85}Se/MoSe_2$ acquired after (a),(b) 1000 CV cycles and 12 h time-overpotential test in 1 M KOH, and (c),(d) 1000 CV cycles and 80 h time-overpotential test in the alkaline simulated water, respectively.

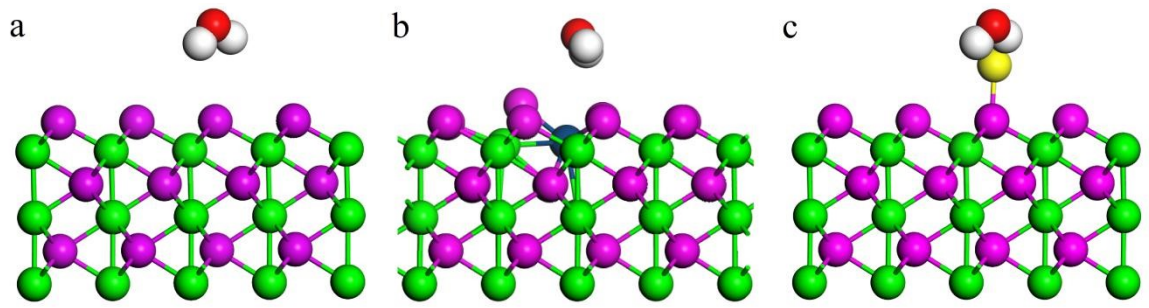

Figure S22. Schematic diagram for H_2O absorption on the NiSe, Mo-NiSe, and NiSe+Cl, respectively.

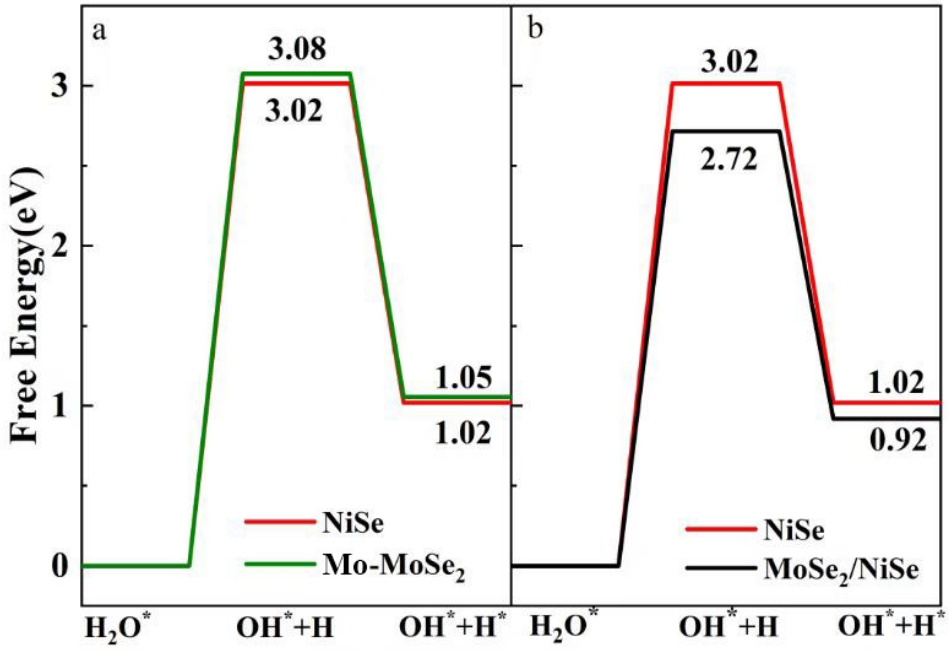

Figure S23. Energy barriers of water decomposition on NiSe, Mo-NiSe, and $MoSe_2$/NiSe. The H_2O*, OH*+H, and OH*+H* represent the initial state, transition state, and final state, respectively. The " * " refers to the chemical group absorbing on the catalyst surface.

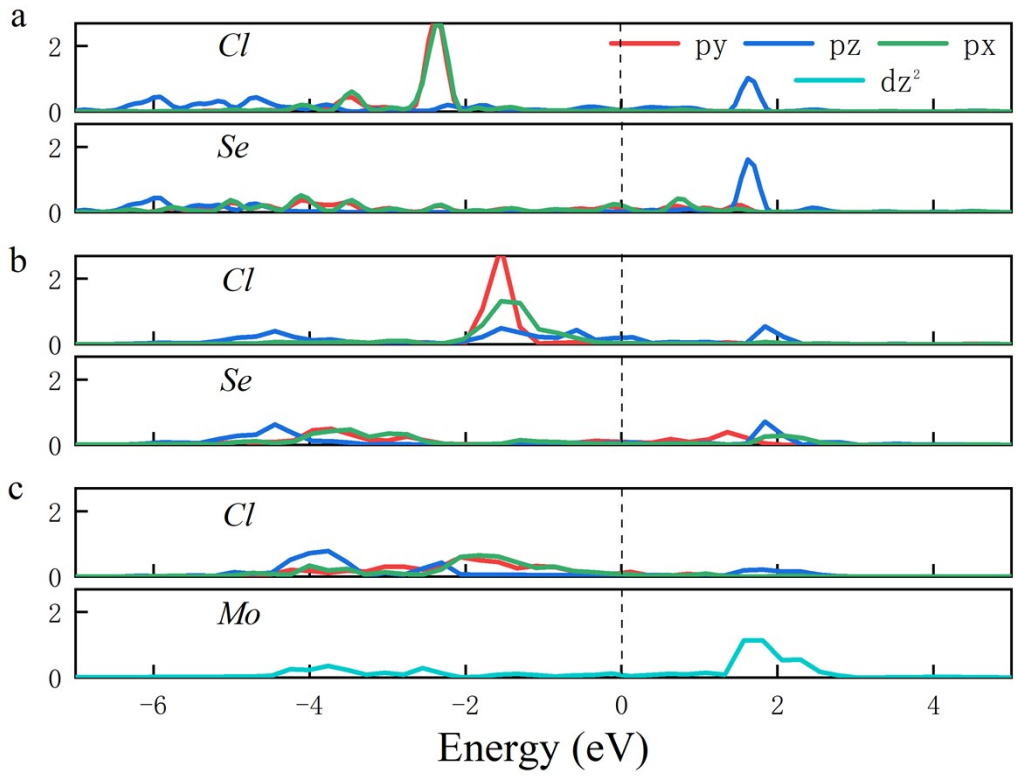

Figure S24. PDOS of Cl adatom and its bonding atom in (**a**) NiSe+Cl, (**b**) Mo-NiSe+Cl_1, and (**c**) Mo-NiSe+Cl_2.

Table S1. The comparison HER performance with reported works.

catalyst	Overpotential (η_{10}/mV)	Tafel spole (mV/dec)	C_{dl} (mF/cm^2)	Stability (h)	electrolyte	Reference
Mo_x-$Ni_{0.85}Se/MoSe_2$	**110 mV**	**70.12 mV/dec**	**92.97 mF/cm^2**	**12 h**	**1 M KOH**	**This work**
P-$NiSe_2$/$MoSe_2$(1-1)@CC	175 mV	78 mV/dec	14.5 mF/cm^2	20 h	1 M KOH	[8]
$Ni_{0.85}Se/Ni_3S_2$	145 mV	130 mV/dec	36.8 mF/cm^2	20 h	1 M KOH	[9]
NF@Mo-$Ni_{0.85}Se$	130 mV	98.98 mV/dec	63.86 mF/cm^2	12 h	1 M KOH	[10]
1T-$MoSe_2$/NiSe NS/NW	120 mV	86 mV/dec	21.2 mF/cm^2	10 h	1 M KOH	[11]
$Ni(OH)_2$-$MoSe_2$	130 mV	78.2 mV/dec	32.3 mF/cm^2	36 h	1 M KOH	[12]
$CoSe_2$-$MoSe_2$(1–1)/rGO	182 mV	89 mV/dec	14.0 mF/cm^2	15 h	1 M KOH	[13]
Mo@(2H-1T)-$MoSe_2$	244 mV(η_{20})	80 mV/dec	91.5 m/ cm^2	12h	1 M KOH	[14]
$MoSe_2$/CoSe hollow spheres	165 mV	82 mV/dec	78.6 mF/cm^2	20h	1 M KOH	[15]
$NiSe_2/Ni_3Se_4$/NF-4	145 mV	69.7 mV/dec	4.4 mF/cm^2	CV2000	1 M KOH	[16]
Mo_x-$Ni_{0.85}Se/MoSe_2$	**110 mV**	**86.19 mv/dec**	**83.07 mF/cm^2**	**80 h**	**1 M KOH + 0.5 M NaCl**	**This work**
oct_Cu_2O/NF	237 mV(η_{20})	90 mv/dec	--	20 h	1 M KOH + 0.5 M NaCl	[17]
$(Co,Fe)PO_4$	134 mV	--	--	--	1 M KOH + 0.5M NaCl	[18]
Ti@NiB-1.5 h	149 mV	118 mV/dec	89.7 mF/cm^2	28 h	1 M KOH + 0.5 M NaCl	[19]
NiFe LDH/FeOOH	181.8 mV	--	--	--	1 M KOH + 0.5 M NaCl	[20]
CoFeZr/NF	159 mV	132.7 mV/dec	--	35 h	1 M KOH + 0.5 M NaCl	[21]
GO@Fe@Ni-Co@NF	150 mV	--	--	--	1 M KOH + 0.5 M NaCl	[22]
Ni_3S_2 @Ni foam	109 mV	52 mV/dec	7.1 mF/cm^2	50 h	1 M KOH + 0.5 M NaCl	[23]
NiFe-PBA-gel-cal	480 mV(η_{100})	160.8 mV/dec	--	60 h	1 M KOH +	[24]

					0.5 M NaCl	
NiCoP/NiCo-LDH	213 mV(η_{50})	65 mV/dec	--	--	1 M KOH + 0.5M NaCl	25
HCl-c-NiFe	175 mV(η_{100})	--	--	300 h	1 M KOH + 0.5 M NaCl	26
NiMoN@NiFeN	82 mV(η_{100})	--	--	48 h	1 M KOH + 0.5 M NaCl	27
$CoSe/MoSe_2$	164 mV	--	--	38 h	1 M KOH + 0.5 M NaCl	28
NiP_x@HA	52 mV	83.76 mV/dec	68.35 mF/cm^2	960 h	1 M KOH + 0.5 M NaCl	29
(C-Co_2P)	192 mV(η_{1000})	--	--	60 h	1 M KOH + 0.5 M NaCl	30
Ti/TiO_2@NiB_x	91 mV	135.6mV/dec	3.62mF/cm^2	72 h	1 M KOH + 0.5 M NaCl	31
Ru_2P@Ru/CNT	27 mV	--	--	250 h	1 M KOH + 0.5 M NaCl	32
NiFeSP-NT	146 mV		107.3 mF/cm^2	1000 h	1 M KOH + 0.5 M NaCl	33
$Ni_3Bi_2S_2$@NF	157 mV(η_{100})	--	--	12 h	1 M KOH + 0.5 M NaCl	34
NiPS/NF	177 mV(η_{100})	--	--	60 h	1 M KOH + 0.5 M NaCl	35
FeNiP-NPHC	180 mV(η_{100})	101 mV/dec	--	100 h	1 M KOH + 0.5 M NaCl	36
S,P-(Ni,Mo,Fe)OOH/NiMoP/wood aerogel	187 mV(η_{50})	--	--	30 h	1 M KOH + 0.5 M NaCl	37
FeP@CoP/NF	205 mV(η_{100})	--	--	100 h	1 M KOH + 0.5 M NaCl	38
S-$NiMoO_4$@NiFe-LDH NS	220 mV(η_{100})	69 mV/dec	148.56 mF/cm^2	20 h	1 M KOH + 0.5 M NaCl	39
Co-Fe_2P	221 mV(η_{100})	--	--	20 h	1 M KOH + 0.5 M NaCl	40
Cu_3P-FeP@CC	178 mV	76.8 mV/dec	--	5 h	1 M KOH + 0.5 M NaCl	41
Ni_3N/Co_4N	282 mV	95 mV/dec	--	14 h	1 M KOH + 0.5 M NaCl	42

Ni-MoN	29 mV	36.8 mV/dec	--	200 h	1 M KOH seawater	[43]
MnCo/NiSe/NF	31.4 mV	58.24 mV/dec	--	200 h	1 M KOH seawater	[44]
1D-Cu@Co-CoO/Rh	137.7 mV	124.8 mV/dec	4.53 mF/cm^2	20 h	1 M KOH seawater	[45]
Ni_3N@C/NF	142 mV(η_{100})	--	--	100 h	1 M KOH seawater	[46]
Ni-SN@C	23 mV	--	--	40 h	1 M KOH seawater	[47]
O-POCs	197 mV	67.6 mV/dec	--	20 h	1 M KOH seawater	[48]
Co-N,P-HCS	287 mV(η_{100})	109 mV/dec	--	100 h	1 M KOH seawater	[49]
Cu_2S thin films	358 mV(η_{100})	128 mV/dec	--	12 h	1 M KOH seawater	[50]
Ni-SA/NC	290 mV(η_{100})	123 mV/dec	--	14 h	1 M KOH seawater	[51]
Mn-doped Ni_2P/Fe_2P	308 mV(η_{100})	--	--	200 h	1 M KOH seawater	[52]
CuS	199 mV	168.14 mV/dec	28.97 mF/cm^2	10 h	1 M KOH seawater	[53]
Ni_2P-Fe_2P/NF	252 mV(η_{100})	--	--	36 h	1 M KOH seawater	[54]
$CoSe_2$-NCF	134 mV	67 mV/dec	--	50 h	1 M KOH seawater	[55]

Supplementary References

1. G. Kresse and J. Furthmuller, Efficient iterative schemes for ab initio total-energy calculations using a plane-wave basis set, *Phys Rev B Condens Matter*, 1996, **54**, 11169-11186.
2. G. Kresse and J. Hafner, Ab initio molecular dynamics for liquid metals, *Phys Rev B Condens Matter*, 1993, **47**, 558-561.
3. G. Kresse and D. Joubert, From ultrasoft pseudopotentials to the projector augmented-wave method, *Physical review b*, 1999, **59**, 1758.
4. J. P. Perdew, K. Burke and M. Ernzerhof, Generalized gradient approximation made simple, *Physical review letters*, 1996, **77**, 3865.
5. P. E. Blöchl, Projector augmented-wave method, *Physical review B*, 1994, **50**, 17953.
6. L. Bengtsson, Dipole correction for surface supercell calculations, *Physical Review B*, 1999, **59**, 12301.
7. J. Neugebauer and M. Scheffler, Adsorbate-substrate and adsorbate-adsorbate interactions of Na and K adlayers on Al(111), *Phys Rev B Condens Matter*, 1992, **46**, 16067-16080.
8. M. Zhu, Q. Yan, Y. Q. Xue, Y. D. Yan, K. Zhu, K. Ye, J. Yan, D. X. Cao, H. J. Xie and G. L. Wang, Free-standing P-doped $NiSe_2$/$MoSe_2$ catalyst for efficient hydrogen evolution in acidic and alkaline media, *ACS Sustainable Chemistry & Engineering*, 2021, **10**, 279-287.
9. D. D. Shi, L. Q. Wu, Q. Chen, D. Y. Jin, M. Y. Chen, Q. Shan and D. H. Wang, Interface engineering of $Ni_{0.85}Se$/Ni_3S_2 nanostructure for highly enhanced hydrogen evolution in alkaline solution, *International Journal of Hydrogen Energy*, 2022, **47**, 305-313.
10. C. M. Yang, C. T. Wang, L. H. Zhou, W. Duan, Y. Y. Song, F. C. Zhang, Y. Z. Zhen, J. J. Zhang, W. W. Bao and Y. X. Lu, Refining d-band center in $Ni_{0.85}Se$ by Mo doping: A strategy for boosting hydrogen generation via coupling electrocatalytic oxidation 5-hydroxymethylfurfural, *Chemical Engineering Journal*, 2021, **422**, 130125.
11. X. Zhang, Y. Y. Zhang, Y. Zhang, W. J. Jiang, Q. H. Zhang, Y. G. Yang, L. Gu, J. S. Hu and L. J. Wan, Phase-controlled synthesis of 1T-$MoSe_2$/NiSe heterostructure nanowire arrays via electronic injection for synergistically enhanced hydrogen evolution, *Small Methods*, 2019, **3**, 1800317.
12. L. M. Zhang, W. F. Zhang, M. L. Wang, H. Wang, J. H. Zang, W. X. Shen, X. W. Huang, D. Z. Kong, Y. T. Tian and T. T. Xu, Interface engineering of nickel Hydroxide-Molybdenum diselenide nanosheet heterostructure arrays for efficient alkaline hydrogen production, *Journal of Colloid and Interface Science*, 2022, **614**, 267-276.
13. M. Zhu, Q. Yan, X. J. Bai, H. Cai, J. Zhao, Y. D. Yan, K. Zhu, K. Ye, J. Yan and D. X. Cao, Construction of reduced graphene oxide coupled with $CoSe_2$-$MoSe_2$ heterostructure for enhanced electrocatalytic hydrogen production, *Journal of Colloid and Interface Science*, 2022, **608**, 922-930.
14. C. M. Yang, L. H. Zhou, C. T. Wang, W. Duan, L. Zhang, F. C. Zhang, J. J. Zhang, Y. Z. Zhen, L. J. Gao and F. Fu, Large-scale synthetic Mo@(2H-1T)-$MoSe_2$ monolithic electrode for efficient hydrogen evolution in all pH scale ranges and seawater, *Applied Catalysis B: Environmental*, 2022, **304**, 120993.
15. J. B. Huang, Y. Jiang, T. Meng, L. Li and M. H. Cao, Regulating electronic structure and adsorptivity in molybdenum selenide for boosting electrocatalytic water splitting, *Electrochimica Acta*, 2021, **390**, 138888.
16. L. Tan, J. T. Yu, H. Y. Wang, H. T. Gao, X. E. Liu, L. Wang, X. L. She and T. R. Zhan, Controllable synthesis and phase-dependent catalytic performance of dual-phase nickel selenides on Ni foam for overall water splitting, *Applied Catalysis B: Environmental*, 2022, **303**, 120915.

17. H. Wang, J. Ying, Y. X. Xiao, J. B. Chen, J. H. Li, Z. Z. He, H. J. Yang and X. Y. Yang, Ultrafast synthesis of Cu_2O octahedrons inlaid in Ni foam for efficient alkaline water/seawater electrolysis, *Electrochemistry Communications*, 2022, **134**, 107177.
18. C. Kim, S. Lee, S. H. Kim, J. Park, S. Kim, S. H. Kwon, J. S. Bae, Y. S. Park and Y. Kim, Cobalt–iron–phosphate hydrogen evolution reaction electrocatalyst for solar-driven alkaline seawater electrolyzer, *Nanomaterials*, 2021, **11**, 2989.
19. Y. R. Zhang, C. Y. Fu, J. L. Fan, H. Y. Lv and W. J. Hao, Preparation of Ti@ NiB electrode via electroless plating toward high-efficient alkaline simulated seawater splitting, *Journal of Electroanalytical Chemistry*, 2021, **901**, 115761.
20. K. Jiang, W. J. Liu, W. Lai, M. L. Wang, Q. Li, Z. L. Wang, J. J. Yuan, Y. L. Deng, J. Bao and H. B. Ji, NiFe layered double hydroxide/FeOOH heterostructure nanosheets as an efficient and durable bifunctional electrocatalyst for overall seawater splitting, *Inorganic chemistry*, 2021, **60**, 17371-17378.
21. W. J. Liu, K. Jiang, Y. M. Hu, Q. Li, Y. L. Deng, J. Bao and Y. C. Lei, Zr-doped CoFe-layered double hydroxides for highly efficient seawater electrolysis, *Journal of Colloid and Interface Science*, 2021, **604**, 767-775.
22. A. R. Jadhav, A. Kumar, J. Lee, T. Yang, S. Na, J. Lee, Y. G. Luo, X. H. Liu, Y. Hwang and Y. Liu, Stable complete seawater electrolysis by using interfacial chloride ion blocking layer on catalyst surface, *Journal of Materials Chemistry A*, 2020, **8**, 24501-24514.
23. Y. C. Li, X. Y. Wu, J. P. Wang, H. X. Wei, S. Y. Zhang, S. L. Zhu, Z. Y. Li, S. L. Wu, H. Jiang and Y. Q. Liang, Sandwich structured Ni_3S_2-MoS_2-Ni_3S_2@ Ni foam electrode as a stable bifunctional electrocatalyst for highly sustained overall seawater splitting, *Electrochimica Acta*, 2021, **390**, 138833.
24. H. Zhang, S. Y. Geng, M. Ouyang, H. Yadegari, F. Xie and D. J. Riley, A self-reconstructed bifunctional electrocatalyst of pseudo-amorphous nickel carbide@ iron oxide network for seawater splitting, *Advanced Science*, 2022, **9**, 2200146.
25. Y. H. Wu, Z. N. Tian, S. F. Yuan, Z. Y. Qi, Y. R. Feng, Y. F. Wang, R. Huang, Y. L. Zhao, J. H. Sun and W. Zhao, Solar-driven self-powered alkaline seawater electrolysis via multifunctional earth-abundant heterostructures, *Chemical Engineering Journal*, 2021, **411**, 128538.
26. S. Duan, Z. Liu, H. H. Zhuo, T. Y. Wang, J. Y. Liu, L. Wang, J. S. Liang, J. T. Han, Y. H. Huang and Q. Li, Hydrochloric acid corrosion induced bifunctional free-standing NiFe hydroxide nanosheets towards high-performance alkaline seawater splitting, *Nanoscale*, 2020, **12**, 21743-21749.
27. L. Yu, Q. Zhu, S. W. Song, B. McElhenny, D. Z. Wang, C. Z. Wu, Z. J. Qin, J. M. Bao, Y. Yu and S. Chen, Non-noble metal-nitride based electrocatalysts for high-performance alkaline seawater electrolysis, *Nature communications*, 2019, **10**, 5106.
28. J. P. Sun, J. Li, Z. Z. Li, C. H. Li, G. M. Ren, Z. S. Zhang and X. C. Meng, Modulating the electronic structure on cobalt sites by compatible heterojunction fabrication for greatly improved overall water/seawater electrolysis, *ACS Sustainable Chemistry & Engineering*, 2022, **10**, 9980-9990.
29. C. Y. Fu, W. J. Hao, J. L. Fan, Q. Zhang, Y. H. Guo, J. C. Fan, Z. L. Chen and G. S. Li, Fabrication of Ultra-Durable and Flexible NiP_x-Based Electrode toward High-Efficient Alkaline Seawater Splitting at Industrial Grade Current Density, *Small*, 2023, **19**, 2205689.
30. W. C. Xu, G. L. Fan, S. L. Zhu, Y. Q. Liang, Z. D. Cui, Z. Y. Li, H. Jiang, S. L. Wu and F. Y. Cheng, Electronic structure modulation of nanoporous cobalt phosphide by carbon doping for alkaline hydrogen evolution reaction, *Advanced Functional Materials*, 2021, **31**, 2107333.

31. C. Y. Fu, S. Weng, J. L. Fan, Y. R. Zhang, Y. H. Guo and W. J. Hao, Boron-based materials modified on the surface of TiO_2 nanorods via electroless plating toward high-efficient solar-driven water splitting, *Chemical Engineering Journal*, 2022, **430**, 132881.
32. D. Zhang, H. F. Miao, X. K. Wu, Z. C. Wang, H. Zhao, Y. Shi, X. L. Chen, Z. Y. Xiao, J. P. Lai and L. Wang, Scalable synthesis of ultra-small Ru_2P@ Ru/CNT for efficient seawater splitting, *Chinese Journal of Catalysis*, 2022, **43**, 1148-1155.
33. F. Nie, Z. Li, X. P. Dai, X. L. Yin, Y. H. Gan, Z. H. Yang, B. Q. Wu, Z. T. Ren, Y. H. Cao and W. Y. Song, Interfacial electronic modulation on heterostructured NiSe@ CoFe LDH nanoarrays for enhancing oxygen evolution reaction and water splitting by facilitating the deprotonation of OH to O, *Chemical Engineering Journal*, 2022, **431**, 134080.
34. D. X. Yao, W. J. Hao, S. Weng, M. L. Hou, W. L. Cen, G. S. Li, Z. L. Chen and Y. T. Li, Local photothermal effect enabling $Ni_3Bi_2S_2$ nanoarray efficient water electrolysis at large current density, *Small*, 2022, **18**, 2106868.
35. H. Y. Wang, J. T. Ren, L. Wang, M. L. Sun, H. M. Yang, X. W. Lv and Z. Y. Yuan, Synergistically enhanced activity and stability of bifunctional nickel phosphide/sulfide heterointerface electrodes for direct alkaline seawater electrolysis, *Journal of Energy Chemistry*, 2022, **75**, 66-73.
36. Q. P. Yu, X. B. Liu, G. S. Liu, X. P. Wang, Z. J. Li, B. Li, Z. X. Wu and L. Wang, Constructing Three-Phase Heterojunction with 1D/3D Hierarchical Structure as Efficient Trifunctional Electrocatalyst in Alkaline Seawater, *Advanced Functional Materials*, 2022, **32**, 2205767.
37. H. J. Chen, Y. H. Zou, J. Li, K. W. Zhang, Y. Z. Xia, B. Hui and D. J. Yang, Wood aerogel-derived sandwich-like layered nanoelectrodes for alkaline overall seawater electrosplitting, *Applied Catalysis B: Environmental*, 2021, **293**, 120215.
38. C. J. Lyu, J. R. Cheng, K. L. Wu, J. W. Wu, N. Wang, Z. L. Guo, P. F. Hu, W. M. Lau and J. L. Zheng, Interfacial electronic structure modulation of CoP nanowires with FeP nanosheets for enhanced hydrogen evolution under alkaline water/seawater electrolytes, *Applied Catalysis B: Environmental*, 2022, **317**, 121799.
39. H. Y. Wang, L. Y. Chen, L. Tan, X. Liu, Y. H. Wen, W. G. Hou and T. R. Zhan, Electrodeposition of NiFe-layered double hydroxide layer on sulfur-modified nickel molybdate nanorods for highly efficient seawater splitting, *Journal of Colloid and Interface Science*, 2022, **613**, 349-358.
40. S. H. Wang, P. Yang, X. F. Sun, H. L. Xing, J. Hu, P. Chen, Z. T. Cui, W. K. Zhu and Z. J. Ma, Synthesis of 3D heterostructure Co-doped Fe_2P electrocatalyst for overall seawater electrolysis, *Applied Catalysis B: Environmental*, 2021, **297**, 120386.
41. C. L. Chai, J. Y. Yang, C. Jiang, L. Liu and J. Y. Xi, Efficient and Durable Cu_3P-FeP for Hydrogen Evolution from Seawater with Current Density Exceeding 1 A cm–2, *ACS Applied Energy Materials*, 2022, **5**, 2909-2917.
42. L. X. Zhang, H. Wei, H. F. Jiu, C. L. Wang, Y. Q. Qin, S. C. Che, Z. X. Guo and Y. X. Han, Ni_3N/Co_4N nanosheet heterojunction electrocatalyst for hydrogen evolution reaction in alkaline fresh water/simulated seawater, *Dalton Transactions*, 2022, **51**, 16733-16739.
43. L. B. Wu, F. H. Zhang, S. W. Song, M. H. Ning, Q. Zhu, J. Q. Zhou, G. H. Gao, Z. Y. Chen, Q. C. Zhou and X. X. Xing, Efficient alkaline water/seawater hydrogen evolution by a nanorod-nanoparticle-structured Ni-MoN catalyst with fast water-dissociation kinetics, *Advanced Materials*, 2022, **34**, 2201774.
44. R. Andaveh, A. S. Rouhaghdam, J. Ai, M. Maleki, K. Wang, A. Seif, G. B. Darband and J. Y. Li, Boosting the electrocatalytic activity of NiSe by introducing MnCo as an

efficient heterostructured electrocatalyst for large-current-density alkaline seawater splitting, *Applied Catalysis B: Environmental*, 2023, **325**, 122355.
45. P. K. L. Tran, D. T. Tran, D. Malhotra, S. Prabhakaran, D. H. Kim, N. H. Kim and J. H. Lee, Highly effective freshwater and seawater electrolysis enabled by atomic Rh-modulated Co-CoO lateral heterostructures, *Small*, 2021, **17**, 2103826.
46. B. R. Wang, M. J. Lu, D. Chen, Q. Zhang, W. W. Wang, Y. T. Kang, Z. X. Fang, G. S. Pang and S. H. Feng, Ni_xFe_yN@ C microsheet arrays on Ni foam as an efficient and durable electrocatalyst for electrolytic splitting of alkaline seawater, *Journal of Materials Chemistry A*, 2021, **9**, 13562-13569.
47. H. Y. Jin, X. S. Wang, C. Tang, A. Vasileff, L. Q. Li, A. Slattery and S. Z. Qiao, Stable and highly efficient hydrogen evolution from seawater enabled by an unsaturated nickel surface nitride, *Advanced Materials*, 2021, **33**, 2007508.
48. S. Li, Z. Y. Zhao, T. Ma, P. Pachfule and A. Thomas, Superstructures of Organic-Polyoxometalate Co-crystals as Precursors for Hydrogen Evolution Electrocatalysts, *Angewandte Chemie International Edition*, 2022, **61**, e202112298.
49. X. K. Wang, X. K. Zhou, C. Li, H. X. Yao, C. H. Zhang, J. Zhou, R. Xu, L. Chu, H. L. Wang and M. Gu, Asymmetric Co-N_3P_1 Trifunctional Catalyst with Tailored Electronic Structures Enabling Boosted Activities and Corrosion Resistance in an Uninterrupted Seawater Splitting System, *Advanced Materials*, 2022, **34**, 2204021.
50. T. Marimuthu, R. Yuvakkumar, P. S. Kumar, G. Ravi, X. Xu, D. Velauthapillai and N. V. Dai Viet, Cost effective and facile low temperature hydrothermal fabrication of Cu_2S thin films for hydrogen evolution reaction in seawater splitting, *International Journal of Hydrogen Energy*, 2022, **47**, 30819-30829.
51. W. J. Zang, T. Sun, T. Yang, S. B. Xi, M. Waqar, Z. K. Kou, Z. Y. Lyu, Y. P. Feng, J. Wang and S. J. Pennycook, Efficient hydrogen evolution of oxidized Ni-N_3 defective sites for alkaline freshwater and seawater electrolysis, *Advanced Materials*, 2021, **33**, 2003846.
52. Y. Z. Luo, P. Wang, G. X. Zhang, S. S. Wu, Z. S. Chen, H. Ranganathan, S. H. Sun and Z. C. Shi, Mn-doped nickel–iron phosphide heterointerface nanoflowers for efficient alkaline freshwater/seawater splitting at high current densities, *Chemical Engineering Journal*, 2023, **454**, 140061.
53. T. Marimuthu, R. Yuvakkumar, G. Ravi, X. Q. Xu, G. Xu and D. Velauthapillai, Hydrothermal construction of flower-like CuS microsphere electrocatalysts for hydrogen evolution reactions in alkaline fresh water, alkaline seawater, and seawater, *International Journal of Energy Research*, 2022, **46**, 19723-19736.
54. L. B. Wu, L. Yu, F. H. Zhang, B. McElhenny, D. Luo, A. Karim, S. Chen and Z. F. Ren, Heterogeneous bimetallic phosphide Ni_2P-Fe_2P as an efficient bifunctional catalyst for water/seawater splitting, *Advanced Functional Materials*, 2021, **31**, 2006484.
55. H. H. Chen, S. S. Zhang, Q. Liu, P. Yu, J. Luo, G. Z. Hu and X. J. Liu, $CoSe_2$ nanocrystals embedded into carbon framework as efficient bifunctional catalyst for alkaline seawater splitting, *Inorganic Chemistry Communications*, 2022, **146**, 110170.